ENSO-conditioned evolution of global mean surface temperature

Michael K. Tippett[1] **and Emily J. Becker**[2]

[1]Department of Applied Physics and Applied Mathematics, Columbia University, New York, New York
[2]Rosenstiel School of Marine, Atmospheric, and Earth Science, University of Miami, Miami, Florida

Key Points:

- A simple regression model was developed to represent the delayed response of global mean surface temperature to ENSO
- The model associates a 1°C December Niño-3.4 anomaly with global mean temperature increases of 0.03°C in summer and 0.11°C in late winter
- Initialized climate forecasts show similar ENSO–temperature links and provide additional value prior to the ENSO peak

Corresponding author: Michael K. Tippett, mkt14@columbia.edu

Abstract

Here we examined how the June–May trajectory of global mean surface temperature (GMST) can be anticipated from recent GMST evolution and upcoming boreal winter Niño-3.4 values. Principal component analysis and dimension reduction of the data led to a simple, interpretable model in which the June–May monthly GMST trajectory is conditioned on two quantities: the average GMST of the prior 12 months and the upcoming December value of Niño-3.4. Including ENSO improves performance relative to persistence baselines that do not include ENSO, especially during the time of the year when atmospheric bridge mechanisms are active. The model associates a December Niño-3.4 anomaly of 1°C with a GMST increase of about 0.03°C during June–August followed by a peak increase of about 0.11°C in the following February. Initialized climate forecasts show broadly similar ENSO–GMST relationships and provide additional skill prior to the ENSO peak.

Plain Language Summary

Global mean surface temperature (GMST) is changing due to anthropogenic and natural forcing, as well as natural variability, with El Niño-Southern Oscillation (ENSO) being the dominant component of natural variability. In this study, we examined how the June-to-May evolution of global mean temperature can be anticipated from two pieces of information available near the beginning of June: the recent GMST level and the expected state of ENSO over the same June-to-May period. In a regression framework, a December Niño-3.4 anomaly of 1°C is preceded by a GMST increase of about 0.03°C during June–August and followed by an increase of about 0.11°C in February. Initialized climate forecasts showed similar links between ENSO and global mean temperature and add more information before the ENSO peak.

1 Introduction

Global mean surface temperature (GMST) is trending upward due to human-caused increases in greenhouse gases. Superimposed on this upward trend are short-term GMST variations in response to natural forcing (e.g., volcanoes) and internal variability. ENSO is the dominant component of internal variability on seasonal timescales, and its influence on GMST is well established (e.g., Angell, 1981; Trenberth et al., 2002). During warm ENSO conditions (El Niño), GMST tends to be elevated relative to the long-term trend, while during cool ENSO conditions (La Niña), the opposite tends to occur. The increase

in GMST from a strong El Niño can be substantial. For instance, Lean and Rind (2008) attributed about 0.23°C of GMST warming to the 1997 "super" El Niño. More recently, the World Meteorological Organization noted "The most recent El Niño, in 2023–24, was one of the five strongest on record and it played a role in the record global temperatures we saw in 2024" (Raghuraman et al., 2024; World Meteorological Organization, 2026).

Tippett and Becker (2024) found that long-lead forecasts of monthly GMST from the North American Multimodel Ensemble (NMME; Becker et al., 2022; Kirtman et al., 2014) were more skillful than a simple linear trend, depending on the targeted calendar month and lead time. The useful skill (i.e., better than the linear trend) of forecasts targeting May–August was limited to lead times of only a month or two, while forecasts targeting boreal winter months had useful skill as far as 12 months ahead. The dependence of GMST forecast skill on target month and lead time is reminiscent of the ENSO spring predictability barrier. Consistent with that interpretation, when ENSO was removed from NMME forecasts of GMST, most of their useful skill was removed as well, evidence that ENSO was a primary source of skill (Tippett & Becker, 2024).

However, even from an observational perspective, the timing and amplitude of the ENSO influence on monthly GMST remain poorly quantified. For example, given the evolution of an ENSO event, there is no clear quantitative description of the associated month-by-month evolution of GMST. One reason for this gap is that previous GMST–ENSO studies (e.g., Trenberth et al., 2002) have often pooled all months together in their analysis, which obscures the seasonal structure of both ENSO and its influence on GMST. Another reason is that the goal of many studies was to remove ENSO-related variability from GMST in order to better isolate trends and responses to external forcing (Angell, 2000; Lean & Rind, 2008; Foster & Rahmstorf, 2011). For that purpose, they focused on the lag at which the ENSO–GMST correlation is strongest, leaving open the broader question of how ENSO influences the month-by-month evolution of GMST.

This inability to translate ENSO information into GMST responses limits the utility of operational ENSO predictions that are produced monthly by meteorological and climate forecast centers around the world. In early 2026, forecasts of a strong El Niño have led to speculation that it could boost GMST by about 0.2°C (e.g., Keith-Lucas, 2026). While this estimate appears plausible, exactly how a given forecast of ENSO conditions

translates into an expected GMST anomaly is less clear, both in terms of timing and amplitude.

Here, we address this gap by deriving a simple and interpretable regression model that outputs GMST evolution at monthly resolution over a June–May 12-month period, given a forecast of ENSO conditions over the same period. The June–May period was chosen because it approximates the typical ENSO development and decay cycle and because ENSO forecasts initialized after boreal spring have useful skill through the following winter (e.g., L'Heureux et al., 2020). We derived the regression model using observed ENSO evolution, analogous to the perfect-prog framework in weather output statistics (Glahn & Lowry, 1972; W. H. Klein et al., 1959). We then used initialized climate forecasts in two ways. First, we used forecast ENSO information as input to the regression model, allowing us to assess the effect of replacing observed ENSO evolution with forecast ENSO evolution. Second, we used initialized climate forecasts as a dynamical comparison. This comparison allows us to assess whether the ENSO–GMST relationships in the forecasts resemble those inferred from observations, and whether direct initialized forecasts of GMST provide additional predictive information beyond the regression model.

Data sources and methods are described in Section 2. Section 3 develops the regression model, evaluates its performance, and compares it with initialized climate forecasts. A summary and discussion are given in Section 4.

2 Data and Methods

We used monthly data from June 1979 through May 2025, comprising 46 June–May ENSO years. Global mean surface temperature (GMST) was computed as the area-weighted global mean of gridded surface temperature from NOAA GlobalTemp v6.1.0 (Huang et al., 2022). NOAA GlobalTemp uses the current WMO climatological standard normals period, 1991–2020, as the reference period for temperature anomalies. Its 1850–1900 mean is −0.77°C, and this value was subtracted to form the preindustrial anomalies shown in the figures. The Niño-3.4 index was computed from ERSSTv5 (Huang et al., 2017) as the area-weighted sea surface temperature over 5°S–5°N, 170°W–120°W. Anomalies are relative to the 1991–2020 base period. We also made limited use of the relative Niño-3.4 index (L'Heureux et al., 2024).

Forecasts of monthly GMST and the Niño 3.4 index were taken from the North American Multi-Model Ensemble (NMME) database (Kirtman et al., 2014; Becker et al., 2022). We used 1 June initialized forecasts from the seven models currently producing real-time forecasts: RSMAS-CCSM4, RSMAS-CESM1, CanESM5, GEM5.2-NEMO, GFDL-SPEAR, NASA-GEOSS2S, and NCEP-CFSv2. Start dates cover 1 June 1991–1 June 2025. Most forecasts extend 12 months beyond their start date; NASA-GEOSS2S and NCEP-CFSv2 extend nine and ten months, respectively. The multi-model mean was computed by averaging the ensemble means from each model, and the multi-model ensemble consists of all ensemble members from all models.

Principal component analysis (PCA) was applied to monthly anomalies of Niño-3.4 and GMST arranged as 12×46 matrices, with rows corresponding to months and columns to June–May years. Double-centered PCA was applied to the same matrices after also removing June–May means (column averages). We used the convention that principal components (PCs) have unit variance and empirical orthogonal functions (EOFs) carry physical units (DelSole & Tippett, 2022). Reconstructions were formed as products of EOFs and PCs, with removed means added back.

Coefficient of determination (R^2), root-mean-square error (RMSE), and mean-squared-error skill score (MSESS) were used as summary measures of regression model performance. Statistical significance of differences in RMSE was assessed using the Wilcoxon signed-rank and sign tests applied to paired squared errors. Because the RMSE values were computed using the same GMST data, RMSE values for different models are not independent, and an F-test for equality of variances is inappropriate (DelSole & Tippett, 2014).

3 Results

We used a regression framework to quantify the dependence of GMST evolution on ENSO, with ENSO represented by the Niño-3.4 index. We represented evolution using 12-month June–May sequences (trajectories) of GMST and Niño-3.4 values. We accounted for the GMST trend in an autoregressive manner by conditioning on prior values of GMST rather than including explicit time trends or radiative forcing. This approach is appropriate here because the primary goal is to quantify the dependence of GMST

on ENSO, in contrast to studies that focus on trend estimation or the separation of forced and internal variability. This formulation can be expressed as the vector equation:

$$\begin{bmatrix} \mathrm{GMST}_{\mathrm{Jun}} \\ \mathrm{GMST}_{\mathrm{Jul}} \\ \vdots \\ \mathrm{GMST}_{\mathrm{Apr}} \\ \mathrm{GMST}_{\mathrm{May}} \end{bmatrix} (y+1) = \boldsymbol{A}_{12} \begin{bmatrix} \mathrm{GMST}_{\mathrm{Jun}} \\ \mathrm{GMST}_{\mathrm{Jul}} \\ \vdots \\ \mathrm{GMST}_{\mathrm{Apr}} \\ \mathrm{GMST}_{\mathrm{May}} \end{bmatrix} (y) + \boldsymbol{B}_{12} \begin{bmatrix} \text{Niño-3.4}_{\mathrm{Jun}} \\ \text{Niño-3.4}_{\mathrm{Jul}} \\ \vdots \\ \text{Niño-3.4}_{\mathrm{Apr}} \\ \text{Niño-3.4}_{\mathrm{May}} \end{bmatrix} (y+1)\,, \qquad (1)$$

where y indexes June–May years, and the 12×12 coefficient matrices $\boldsymbol{A}_{12}$ and $\boldsymbol{B}_{12}$ represent, respectively, the dependence of a GMST trajectory on its prior values and on the contemporaneous Niño-3.4 trajectory. In addition to quantifying the dependence of GMST on ENSO, this model can be used in a predictive manner to anticipate GMST evolution given a forecast Niño-3.4 trajectory.

The regression model in (1) is high-dimensional with 24 predictors and 12 predictands. The matrices $\boldsymbol{A}_{12}$ and $\boldsymbol{B}_{12}$ together contain 288 coefficients. To avoid overfitting, facilitate interpretation, and reduce the complexity of the model, we applied PCA to the two datasets. PCA is an unsupervised and systematic dimension-reduction method that optimizes explained variance and, as used here, ignores relationships between predictors and predictands. Previous work found that 12-month Niño-3.4 trajectories are well approximated by one or two PCs, both in observations and in seasonal forecasts (Bunge & Clarke, 2009; Tippett & L'Heureux, 2020). Consistent with those results, we found that approximately 95% of the variability of June–May Niño-3.4 segments is explained by the first two PCs (Fig. 1a). Moreover, the same is true of GMST—approximately 95% of the variability of a June–May GMST trajectory is explained by the first two PCs (Fig. 1b).

Although PCA need not yield physically meaningful or readily explainable components, the leading PCs of GMST and Niño-3.4 trajectories admit relatively clear interpretations. EOF1 of Niño-3.4 peaks in December, reflecting the seasonal phase locking of ENSO (Fig. 1a). EOF2 of Niño-3.4 is a dipole in time centered on December. The dipole structure is related to the mathematical requirement that EOF2 be orthogonal to EOF1 and serves to represent shifts of the Niño-3.4 peak away from December. EOF1 of GMST is nearly uniform across months (Fig. 1b), while PC1 of GMST shows a clear

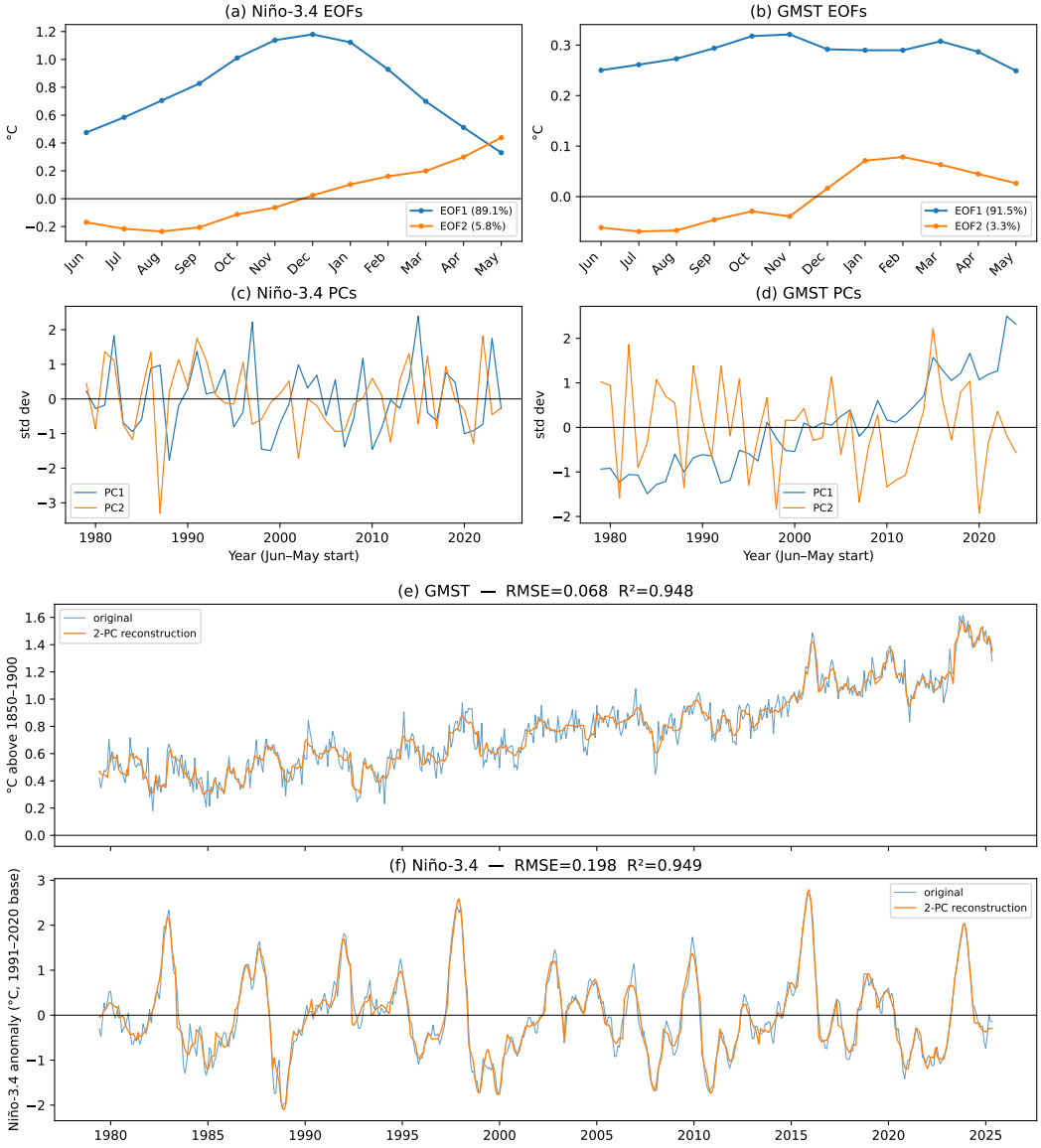

Figure 1. The leading two EOFs of June–May trajectories of (a) Niño-3.4 and (b) global mean surface temperature (GMST). The corresponding leading two PCs of (c) Niño-3.4 and (d) GMST. Two-PC reconstructions of (e) Niño-3.4 and (f) GMST with root mean squared error (RMSE) and R^2 values in the title.

upward trend (Fig. 1d). PC1 of GMST represents the approximately uniform (across calendar months) upward trend of GMST. EOF2 of GMST is negative and roughly uniform over the June–November period until it rises in December and peaks in January and February, while PC2 shows no visible trend. The asymmetry of the dipole structure of EOF2 suggests that it represents the delayed post-peak response of GMST to ENSO via the atmospheric bridge (Alexander et al., 2002; S. A. Klein et al., 1999). Reconstructions of Niño-3.4 and GMST show that 2 EOFs are adequate to capture interannual variability (R^2 values of about 95%; Fig. 1e, f), although more unresolved subannual variability is visible in the GMST time series than in the Niño-3.4 time series because much of the GMST variance is associated with its long-term trend.

The PCA analysis motivates replacing (1) with the four-PC model:

$$\begin{bmatrix} \text{GMST}_{\text{PC1}} \\ \text{GMST}_{\text{PC2}} \end{bmatrix} (y+1) = \boldsymbol{A}_{\text{4-PC}} \begin{bmatrix} \text{GMST}_{\text{PC1}} \\ \text{GMST}_{\text{PC2}} \end{bmatrix} (y) + \boldsymbol{B}_{\text{4-PC}} \begin{bmatrix} \text{Niño-3.4}_{\text{PC1}} \\ \text{Niño-3.4}_{\text{PC2}} \end{bmatrix} (y+1)\,, \qquad (2)$$

where the 2×2 matrices $\boldsymbol{A}_{\text{4-PC}}$ and $\boldsymbol{B}_{\text{4-PC}}$ represent, respectively, the dependence of the first two PCs of GMST on their prior values and on the contemporaneous values of PC1 and PC2 of Niño-3.4. The number of coefficients is now reduced from 288 to eight.

We next examined the simultaneous and lagged correlations of the first two PCs of Niño-3.4 and GMST. The strongest simultaneous correlation is the 0.61 correlation between N34-PC1 and GMST-PC2, which supports our hypothesis that GMST-EOF2 represents the delayed GMST response to ENSO (Fig. 2a). The other simultaneous correlations are weak ($R^2 < 4\%$). The strongest lagged relation between PCs is the 0.92 correlation between GMST-PC1(y) and GMST-PC1($y+1$) which reflects the upward trend in GMST-PC1 and the resulting strong year-to-year persistence (Fig. 2b). In contrast, the lag-1 autocorrelation of GMST-PC2 is small and negative ($r = -0.18$), consistent with the interpretation of GMST-PC2 as an ENSO response with little persistence from one year to the next. The source of the correlation between N34-PC2(y) and N34-PC1($y+1$) is less clear, though it is visually evident in the PC time series (Fig. 1c). It might reflect imperfect alignment of the June–May year with the ENSO life cycle. The correlation between N34-PC2(y) and GMST-PC2(y+1) ($r = 0.37$) is explained almost entirely by the pathway N34-PC2(y) $\rightarrow$ N34-PC1($y+1$) $\rightarrow$ GMST-PC2($y+1$). After accounting for N34-PC1($y+1$), the partial correlation between N34-PC2(y) and GMST-PC2($y+1$) is only 0.04.

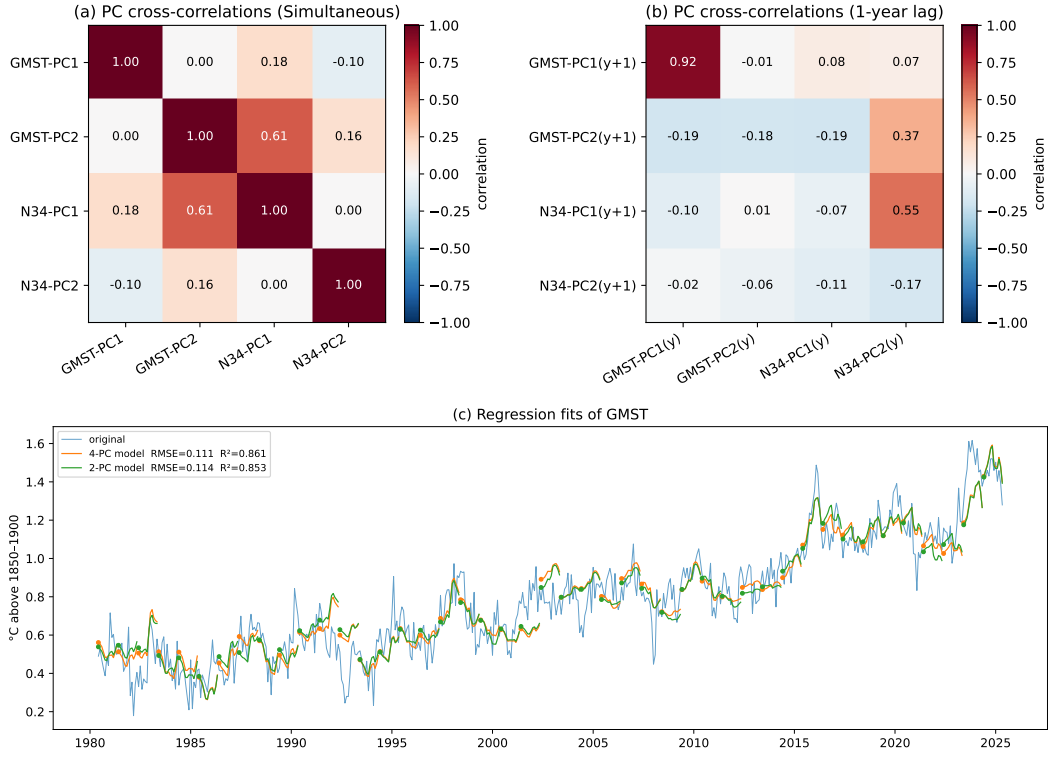

Figure 2. (a) Simultaneous and (b) one-year lag correlations between the first two PCs of Niño-3.4 and global mean surface temperature (GMST). Panel (c) shows the fit of GMST time series by the four-PC model, the two-PC model, and the simplified model (see text for model details). Dots show the start of June–May segments. The RMSE and R^2 of the models are shown in the legend.

The correlation analysis above suggests that little is lost by using only two PCs as predictors: GMST-PC1(y) and N34-PC1($y+1$). The two-PC model is:

$$\begin{bmatrix}\text{GMST}_{\text{PC1}}\\ \text{GMST}_{\text{PC2}}\end{bmatrix}(y+1) = \boldsymbol{A}_{\text{2-PC}}\begin{bmatrix}\text{GMST}_{\text{PC1}}\end{bmatrix}(y) + \boldsymbol{B}_{\text{2-PC}}\begin{bmatrix}\text{Niño-3.4}_{\text{PC1}}\end{bmatrix}(y+1)\,, \quad (3)$$

where the 2×1 matrices $\boldsymbol{A}_{\text{2-PC}}$ and $\boldsymbol{B}_{\text{2-PC}}$ represent, respectively, the dependence of the first two PCs of GMST on the prior value of PC1 of GMST and on the contemporaneous value of PC1 of Niño-3.4. The number of coefficients is reduced from eight to four. The fit obtained with these two predictors is nearly identical to that obtained with four predictors (Fig. 2c), consistent with only the coefficients of GMST-PC1(y) and N34-PC1($y+1$) being large and statistically significant in the four-predictor model (Table S1) and their having nearly the same values in the two-predictor model (Table S2).

While the two-PC predictor model is effective and parsimonious, further simplifications can improve interpretability. In particular, the predictors GMST-PC1(y) and N34-PC1($y+1$) are defined by the PCA itself and depend on the specific data used. Replacing the predictor PCs with quantities that closely approximate them, but whose calculation is more transparent, would yield a more explainable model. Because N34-PC1 is highly correlated ($r > 0.98$) with the December Niño-3.4 value (Fig. 3a), we replaced N34-PC1 with December Niño-3.4. This close correspondence follows from the structure of the leading EOFs: EOF1 peaks in December, while EOF2 is close to zero in December. We replaced GMST-PC1 with the June–May mean GMST, which we refer to as the GMST level. The GMST level is highly correlated with GMST-PC1 ($r > 0.99$; Fig. 3a) because GMST-EOF1 is nearly uniform across months. This replacement suggests an alternative decomposition of GMST in which the first component is simply the level (June–May mean), and the second component captures as much as possible of the remaining variance. We implemented this idea by decomposing each June–May GMST trajectory into its June–May level and departures from that level, and then applying PCA to the departures. Because this decomposition removes both monthly means and June–May means, we call it double-centered PCA. Although double-centered PCA is not variance-optimal, the loss is small: the variance explained by the first two modes decreases from 94.8% to 94.3% (Fig. S1). The leading EOF from the double-centered decomposition is similar to GMST-EOF2 (Fig. 3a), and the corresponding PC is also similar to GMST-PC2, with correlation 0.993 (Fig. 3b).

These replacements (N34-PC1 replaced by December Niño-3.4 and GMST-PC1 replaced by level) give the simplified model:

$$\begin{bmatrix} \mathrm{GMST}_{\mathrm{level}} \\ \mathrm{GMST}_{\mathrm{DC\text{-}PC1}} \end{bmatrix} (y+1) = \boldsymbol{A} \left[\mathrm{GMST}_{\mathrm{level}} \right] (y) + \boldsymbol{B} \left[\mathrm{Niño\text{-}3.4}_{\mathrm{Dec}} \right] (y+1)\,, \qquad (4)$$

where the 2×1 matrices $\boldsymbol{A}$ and $\boldsymbol{B}$ represent, respectively, the dependence of the GMST level and its first DC-PC on the prior value of the GMST level and on the contemporaneous December value of Niño-3.4 (regression summary in Table S3). The performance of the simplified model is nearly identical to that of the two-PC predictor model (Fig. 3c).

An attractive feature of the simplified model is that, once the recent GMST level is specified, the shape of the predicted GMST response is fixed and only its amplitude changes with the December Niño-3.4 value. Figure 3d shows the implied June–May GMST response per +1°C of December Niño-3.4. The response is about 0.03°C during June–August, rises sharply beginning in December, and peaks at about 0.11°C in February. The same analysis using relative Niño-3.4 gives a similar GMST response (Fig. 3d), indicating that the result is not sensitive to the choice of ENSO index. The slightly weaker response obtained with relative Niño-3.4 reflects its larger December variance during this period—about 8% greater than that of the traditional Niño-3.4 index—rather than a weaker correlations with GMST residuals (Fig. S2; Table S4). The simplified model allows statements of the form: "given the recent 12-month average of GMST and the expected December Niño-3.4 value, the June–May GMST trajectory is expected to be . . . ". As an illustration, a June 2025–March 2026 GMST level of 1.27°C and an assumed December 2026 Niño-3.4 value of +2.0°C give a predicted February 2027 peak near 1.5°C above preindustrial.

Having derived the simplified regression model, we next address three important questions: How much is gained by accounting for ENSO? How much does performance change when forecast rather than observed December Niño-3.4 is used? How does the simplified regression model compare with initialized climate forecasts of GMST? This comparison helps determine whether the simplified statistical model captures information already represented in dynamical forecasts, or whether the dynamical forecasts provide additional predictive information. To address the first question, we considered two persistence-only benchmarks: one based on the preceding June–May mean GMST and one based on the preceding May GMST value. To address the second and third ques-

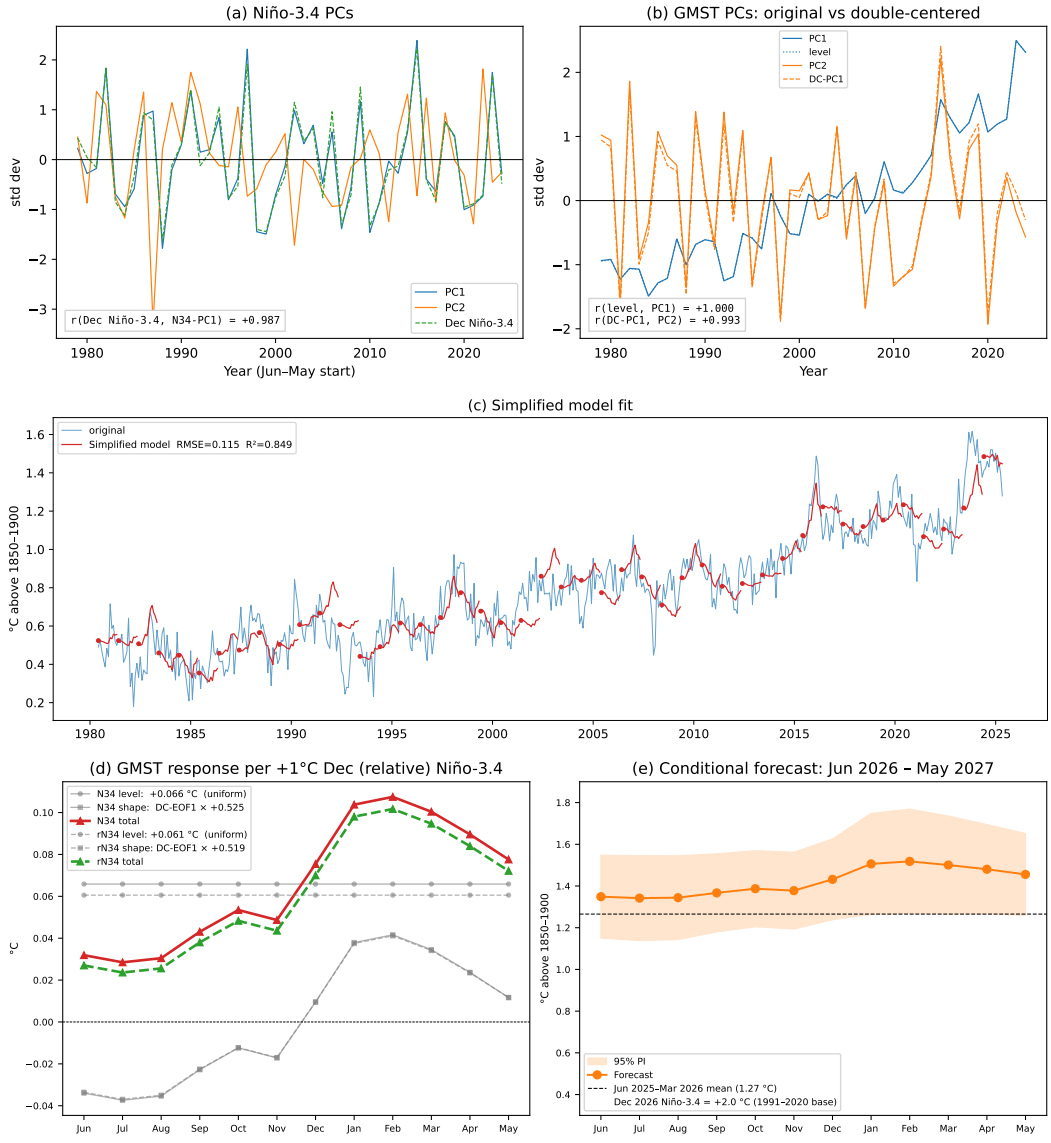

Figure 3. Comparison of (a) PC1 of Niño-3.4 with December Niño-3.4 and comparison of (b) GMST PCs with GMST level and double-centered PC1. Panel (c) shows the fit of GMST time series by the simplified model (see text for details). Panel (g) shows a 2026–27 illustration for December 2026 Niño-3.4 of 2.0°C. Panel (h) shows the implied June–May GMST response per +1°C of December Niño-3.4 and relative Niño-3.4.

tions, we used NMME multimodel-mean forecasts of December Niño-3.4 and monthly GMST.

To compare the simplified regression model with the NMME forecasts, we looked at trends and the relation in the models of December Niño-3.4 with GMST level and GMST DC-PC1. The NMME models broadly reproduce the observed ENSO–GMST relationships, although with notable model differences (Fig. S3; Table S5). Several models have GMST trends that are significantly larger than observed as noted previously (DelSole et al., 2025; Swart et al., 2019; Tippett & Becker, 2024), and CCSM4 has a substantially weaker correlation between December Niño-3.4 and GMST-DC-PC1 than is present in observations. For the correlation between GMST level and December Niño-3.4, CanESM5 and GEM5.2-NEMO are stronger than observed (Fig. S3). These two models also have the most positive December Niño-3.4 trends (Table S5). CCSM4 is weaker than observed, while the remaining models are close to observations. For the relation between GMST-DC-PC1 and December Niño-3.4, CCSM4 is again much weaker than observed ($r = 0.22$ compared with $r = 0.63$). The remaining model correlations are slightly weaker than observed, with the exception of NCEP-CFSv2.

We next assess performance relative to the persistence-only benchmarks. Both the simplified regression model and the NMME forecasts outperform the prior June–May mean benchmark in every month, as measured by RMSE (Fig. 4a). The May-value benchmark is more competitive early in the June–May year, particularly in June and July. Compared with this benchmark, both the simplified model and the NMME forecasts have lower RMSE from August through May. For the simplified regression model, there is little difference between using observed December Niño-3.4 and using forecast December Niño-3.4, and the RMSE differences are not statistically significant (Table S6). The NMME forecasts of GMST have lower RMSE than the simplified model for target months through December, and similar RMSE for later target months. The largest NMME advantage occurs in October, which is the only month for which the difference between the NMME GMST forecast and the simplified model using forecast December Niño-3.4 is statistically significant (Table S6). We computed MSESS using the prior June–May GMST average as the reference forecast (Fig. 4b). The resulting scores show that the simplified model improves most on persistence after December, consistent with the delayed GMST response to ENSO. In contrast, the NMME GMST forecasts show their largest advantage over persistence before December, especially in September and October.

Representative years illustrate these differences (Figs. 4c–h). In cool ENSO years, the simplified model captures the winter cooling and spring rebound but with reduced amplitude, as expected from regression shrinkage. In warm ENSO years, it captures delayed warming, while the NMME forecasts are often closer to the observed level, especially in 2015–16 and 2023–24. The 2023–24 case remains exceptional because the sharp September warming is underestimated by both approaches.

4 Summary and discussion

Here we developed a simple and interpretable regression model that quantifies the relationship between ENSO and global mean surface temperature (GMST). The model allows the June–May evolution of monthly GMST to be anticipated based on information that is available near the beginning of June. We began with a high-dimensional formulation and applied a sequence of systematic, physically motivated simplifications to obtain a model with two predictors. The resulting predictors—recent GMST level and expected December Niño-3.4 value—serve to model the persistence of GMST and its delayed response to ENSO. Principal component analysis (PCA) of 12-month June–May trajectories of GMST and Niño-3.4 was especially useful because the first two PCs of GMST and Niño-3.4 explain more than 95% of the variance of June–May trajectories. The efficiency of PCA in explaining GMST evolution might be expected because a substantial fraction of GMST variance is associated with the long-term trend. The result is more striking for Niño-3.4 evolution, since a common view is that each ENSO event has its own distinct temporal structure.

The structure of the leading EOFs suggested further simplifications to improve interpretability. Since the leading EOF of GMST is nearly uniform across months, it was replaced by the June–May average of GMST. The leading Niño-3.4 EOF represents the typical temporal evolution of ENSO and peaks in December, so the corresponding PC was replaced by the December value of Niño-3.4. These changes simplified the predictors with little loss of accuracy. According to the model, an expected December Niño-3.4 anomaly of 1°C is associated with a GMST increase of about 0.03°C during June–August and a peak increase of about 0.11°C in the following February.

Although the ENSO contribution to GMST is modest, including ENSO improves prediction relative to persistence-only benchmarks. The simplified model reduces RMSE

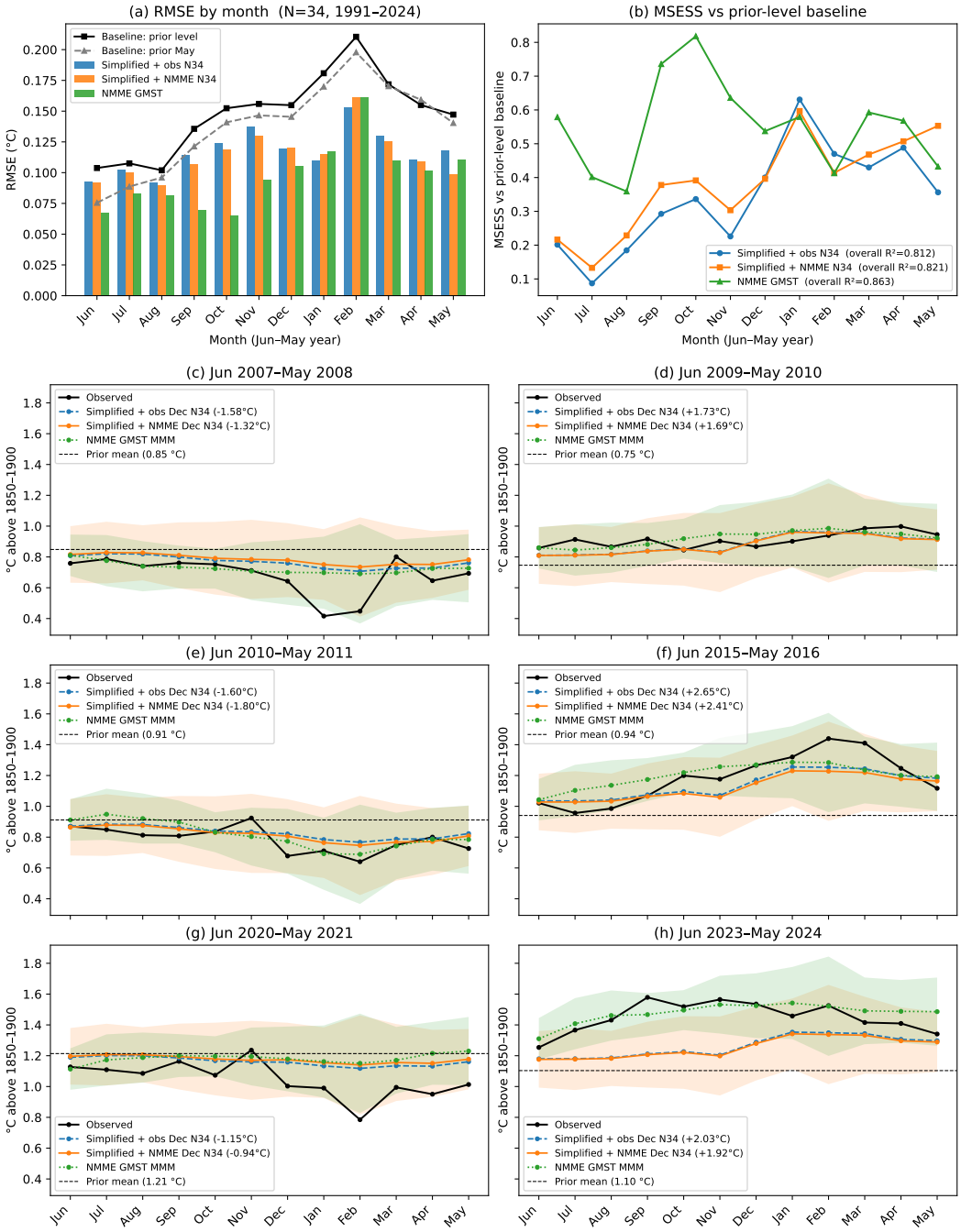

Figure 4. (a) Root-mean squared error (RMSE) of the persistence baselines, the simplified model (using observed and forecast December Niño-3.4), and NMME forecasts of June–May global mean surface temperature (GMST) for the period 1991–2024. (b) Mean-squared error skill score (MSESS) of the simplified model and NMME forecasts relative to the prior June–May GMST level persistence baseline. Observed June–May GMST, simple model fits, and NMME GMST forecasts for (c) 2007–08, (d) 2009–10, (e) 2010–11, (f) 2015–16, (g) 2020–21, and (h) 2023–24.

relative to the prior June–May mean benchmark in every month and relative to the prior May benchmark from August through May. The MSESS results show that this improvement is largest after December, consistent with the delayed GMST response to ENSO. Replacing observed December Niño-3.4 with forecast December Niño-3.4 produces little change in RMSE. By contrast, direct NMME forecasts of GMST show their largest advantage earlier in the June–May year, especially before December.

A broader implication is that ENSO information is most useful for GMST prediction when the forecast target is aligned with the ENSO life cycle. Calendar-year and annual-to-decadal forecast systems are valuable, but their initialization and verification windows are not optimized for taking advantage of post-spring-barrier ENSO predictability to anticipate June–May GMST evolution (Hermanson et al., 2022; World Meteorological Organization, 2025; Dunstone et al., 2024; Folland et al., 2025). Initialized seasonal forecast systems, because they are run monthly, are better positioned to exploit the ENSO signal as it emerges and becomes reliable, although they still have known trend and ensemble-calibration errors (L'Heureux et al., 2022; Tippett & Becker, 2024). Despite these limitations, the NMME multimodel mean provided a useful benchmark here and added skill relative to the simplified regression model during the early part of the June–May forecast year.

Open Research Section

NOAAGlobalTemp version 6.1 data used here are from `https://www.ncei.noaa.gov/data/noaa-global-surface-temperature/v6.1/access/gridded/NOAAGlobalTemp_v6.1.0_gridded_s185001_e202603_c20260406T114628.nc`. The data and URL are updated every month. NOAA Extended Reconstructed SST V5 (ERSSTv5) data are provided by the NOAA PSL, Boulder, Colorado, USA, from their website at `https://downloads.psl.noaa.gov/Datasets/noaa.ersst.v5/sst.mnmean.nc`. Monthly values of the relative Niño-3.4 index are available from `https://www.cpc.ncep.noaa.gov/data/indices/Rnino34.ascii.txt`. NMME data are available from the IRI Data Library `https://iridl.ldeo.columbia.edu/SOURCES/.Models/.NMME/`.

Conflict of Interest

The authors declare no conflicts of interest.

Acknowledgments

We thank Dr. Michelle L. L'Heureux for helpful discussions and suggestions. Support from NSF is acknowledged by EJB (2223262). The authors also acknowledge the use of AI tools, including OpenAI's ChatGPT and Anthropic's Claude, to assist with code and manuscript editing.

References

Alexander, M. A., Bladé, I., Newman, M., Lanzante, J. R., Lau, N.-C., & Scott, J. D. (2002). The atmospheric bridge: The influence of ENSO teleconnections on air—sea interaction over the global oceans. *Journal of Climate*, *15*, 2205–2231. doi: 10.1175/1520-0442(2002)015⟨2205:TABTIO⟩2.0.CO;2

Angell, J. K. (1981). Comparison of variations in atmospheric quantities with sea surface temperature variations in the equatorial eastern Pacific. *Monthly Weather Review*, *109*, 230–243. doi: 10.1175/1520-0493(1981)109⟨0230:COVIAQ⟩2.0.CO;2

Angell, J. K. (2000). Tropospheric temperature variations adjusted for El Niño, 1958–1998. *Journal of Geophysical Research: Atmospheres*, *105*, 11841–11849. doi: 10.1029/2000JD900044

Becker, E. J., Kirtman, B. P., L'Heureux, M., Muñoz, Á. G., & Pegion, K. (2022).

A decade of the North American Multimodel Ensemble (NMME): Research, application, and future directions. *Bulletin of the American Meteorological Society*, *103*, E973–E995. doi: 10.1175/BAMS-D-20-0327.1

Bunge, L., & Clarke, A. J. (2009). A verified estimation of the El Niño index Niño-3.4 since 1877. *Journal of Climate*, *22*, 3979–3992. doi: 10.1175/2009JCLI2724.1

DelSole, T., & Tippett, M. K. (2014). Comparing forecast skill. *Monthly Weather Review*, *142*, 4658–4678. doi: 10.1175/MWR-D-14-00045.1

DelSole, T., Tippett, M. K., & Johnson, N. C. (2025). Diagnosing errors in climate forecast models using forced autoregressive models. *Journal of Advances in Modeling Earth Systems*, *17*, e2024MS004926. doi: 10.1029/2024MS004926

DelSole, T. M., & Tippett, M. K. (2022). *Statistical methods for climate scientists*. Cambridge University Press. doi: 10.1017/9781108659055

Dunstone, N. J., Smith, D. M., Atkinson, C., Colman, A., Folland, C., Hermanson, L., ... others (2024). Will 2024 be the first year that global temperature exceeds 1.5°C? *Atmospheric Science Letters*, *25*, e1254.

Folland, C., Colman, A., Dunstone, N., Smith, D., & Scaife, A. (2025). A review of 25 annual forecasts of global mean surface temperature including the record warm years 2023 and 2024. *Geophysical Research Letters*, *52*, e2025GL117308. doi: 10.1029/2025GL117308

Foster, G., & Rahmstorf, S. (2011). Global temperature evolution 1979–2010. *Environmental Research Letters*, *6*, 044022. doi: 10.1088/1748-9326/6/4/044022

Glahn, H. R., & Lowry, D. A. (1972). The use of model output statistics (MOS) in objective weather forecasting. *J. Appl. Meteor.*, *11*, 1203-1211.

Hermanson, L., Smith, D., Seabrook, M., Bilbao, R., Doblas-Reyes, F., Etienne Tourigny, V. L., ... Kumar, A. (2022). WMO global annual to decadal climate update: a prediction for 2021–25. *Bulletin of the American Meteorological Society*, *103*, E1117–E1129.

Huang, B., Thorne, P. W., Banzon, V. F., Boyer, T., Chepurin, G., Lawrimore, J. H., ... Zhang, H.-M. (2017). Extended reconstructed sea surface temperature, version 5 (ERSSTv5): Upgrades, validations, and intercomparisons. *Journal of Climate*, *30*, 8179–8205. doi: 10.1175/JCLI-D-16-0836.1

Huang, B., Yin, X., Menne, M. J., Vose, R., & Zhang, H.-M. (2022). Improvements

to the land surface air temperature reconstruction in NOAAGlobalTemp: An artificial neural network approach. *Artificial Intelligence for the Earth Systems*, *1*, e220032. doi: 10.1175/AIES-D-22-0032.1

Keith-Lucas, S. (2026, 10). *Is a 'Super El Niño' on the way and how will it affect the UK?* Retrieved from `https://www.bbc.com/weather/articles/cj94nzj33m0o` (Accessed 2026-04-14)

Kirtman, B., Min, D., Infanti, J. M., Kinter, J. L., III, Paolino, D. A., Zhang, Q., ... Wood, E. F. (2014). The North American Multi-Model Ensemble (NMME): Phase-1 seasonal to interannual prediction, Phase-2 toward developing intra-seasonal prediction. *Bulletin of the American Meteorological Society*, *95*, 585–601. doi: 10.1175/BAMS-D-12-00050.1

Klein, S. A., Soden, B. J., & Lau, N.-C. (1999). Remote sea surface temperature variations during ENSO: Evidence for a tropical atmospheric bridge. *Journal of Climate*, *12*, 917–932. doi: 10.1175/1520-0442(1999)012⟨0917:RSSTVD⟩2.0.CO;2

Klein, W. H., Lewis, B. M., & Enger, I. (1959). Objective prediction of five-day mean temperatures during winter. *Journal of Atmospheric Sciences*, *16*, 672–682. doi: 10.1175/1520-0469(1959)016⟨0672:OPOFDM⟩2.0.CO;2

Lean, J. L., & Rind, D. H. (2008). How natural and anthropogenic influences alter global and regional surface temperatures: 1889 to 2006. *Geophysical Research Letters*, *35*. doi: 10.1029/2008GL034864

L'Heureux, M. L., Levine, A., Newman, M., Ganter, C., Luo, J.-J., Tippett, M. K., & Stockdale, T. (2020). ENSO Prediction. In M. McPhaden, A. Santoso, & W. Cai (Eds.), *El Niño-Southern Oscillation (ENSO) in a Changing Climate.* AGU. doi: 10.1002/9781119548164.ch10

L'Heureux, M. L., Tippett, M. K., & Wang, W. (2022). Prediction challenges from errors in tropical Pacific sea surface temperature trends. *Frontiers in Climate*, *4*. doi: 10.3389/fclim.2022.837483

L'Heureux, M. L., Tippett, M. K., Wheeler, M. C., Nguyen, H., Narsey, S., Johnson, N., ... others (2024). A relative sea surface temperature index for classifying ENSO events in a changing climate. *Journal of Climate*, *37*, 1197–1211. doi: 10.1175/JCLI-D-23-0406.1

Raghuraman, S. P., Soden, B., Clement, A., Vecchi, G., Menemenlis, S., & Yang,

W. (2024). The 2023 global warming spike was driven by the El Niño–Southern Oscillation. *Atmospheric chemistry and physics*, *24*, 11275–11283. doi: 10.5194/acp-24-11275-2024

Swart, N., Cole, J., Kharin, V., Lazare, M., Scinocca, J., Gillett, N., ... Jiao, Y. (2019). The Canadian earth system model version 5 (CanESM5. 0.3). *Geoscientific Model Development*, *12*, 4823–4873. doi: 10.5194/gmd-12-4823-2019

Tippett, M. K., & Becker, E. J. (2024). Trends, skill, and sources of skill in initialized climate forecasts of global mean temperature. *Geophysical Research Letters*, *51*, e2024GL110703. doi: https://doi.org/10.1029/2024GL110703

Tippett, M. K., & L'Heureux, M. L. (2020). Low-dimensional representations of Niño 3.4 evolution and the spring persistence barrier. *npj Climate and Atmospheric Science*, *3*, 24. doi: 10.1038/s41612-020-0128-y

Trenberth, K. E., Caron, J. M., Stepaniak, D. P., & Worley, S. (2002). Evolution of El Niño–Southern Oscillation and global atmospheric surface temperatures. *Journal of Geophysical Research: Atmospheres*, *107*, AAC–5. doi: 10.1029/2000JD000298

World Meteorological Organization. (2025, May 28). *WMO Global Annual to Decadal Climate Update 2025–2029.* Retrieved from `https://wmo.int/sites/default/files/2025-05/WMO_GADCU_2025-2029_Final.pdf` (Accessed 2026-04-18)

World Meteorological Organization. (2026, March). *ENSO neutral conditions expected as La Niña fades, but El Niño chances rise.* `https://wmo.int/news/media-centre/enso-neutral-conditions-expected-la-nina-fades-el-nino-chances-rise`. (Accessed: 2026-04-05)

Supporting Information for "ENSO-conditioned evolution of global mean surface temperature"

Michael K. Tippett[1] **and Emily J. Becker**[2]

[1]Department of Applied Physics and Applied Mathematics, Columbia University, New York, New York

[2]Rosenstiel School of Marine, Atmospheric, and Earth Science, University of Miami, Miami, Florida

Contents of this file

1. Figures S1 to S3
2. Tables S1 to S6

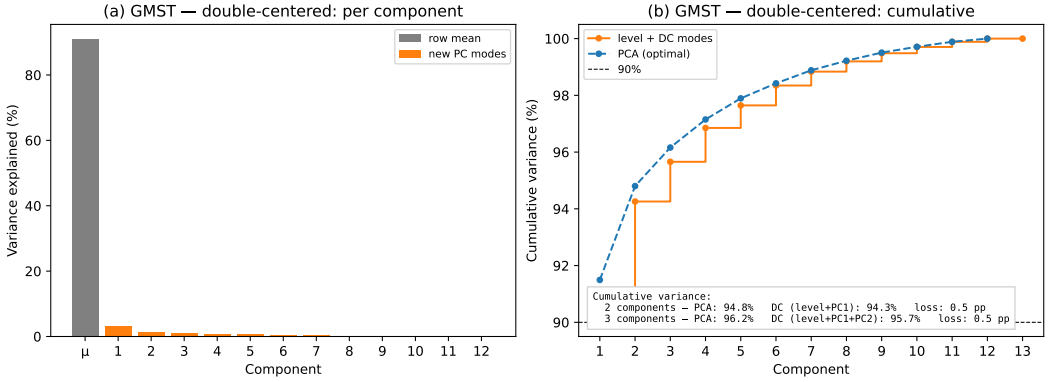

Figure S1. Variance per mode and cumulative variance for double-centered PCA.

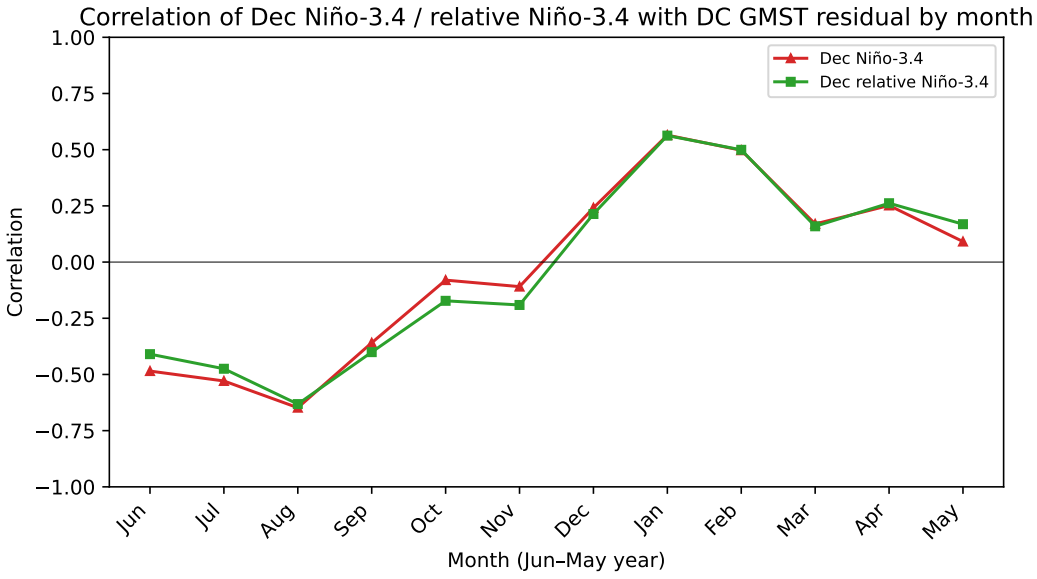

Figure S2. December Niño-3.4 and relative December Niño-3.4 correlations with DC GMST residuals (level removed) by month.

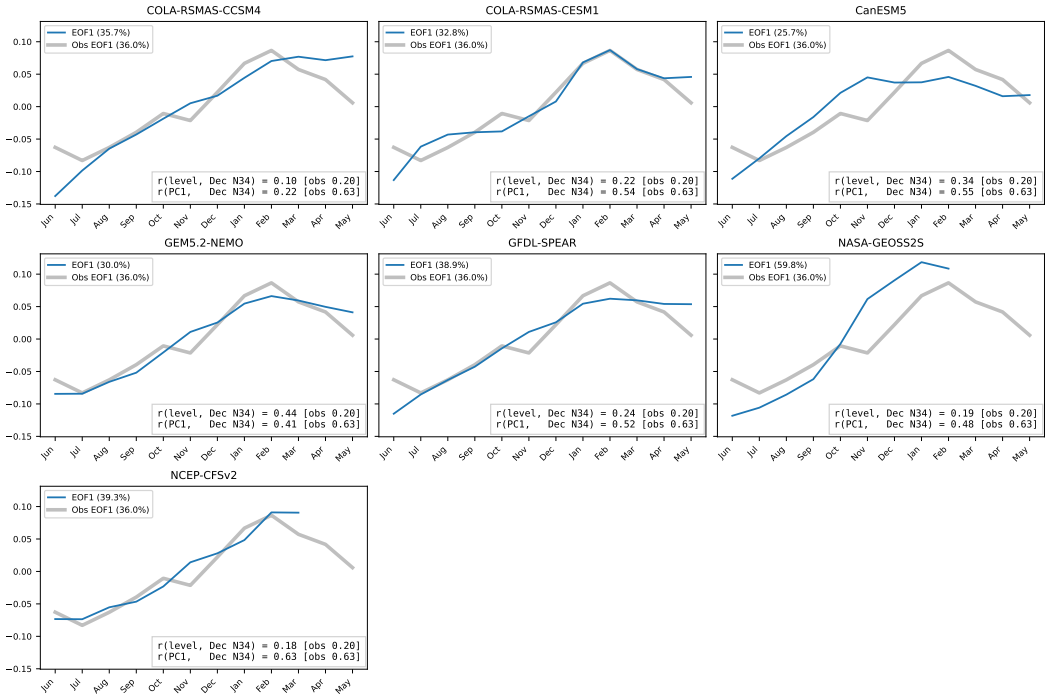

Figure S3. The first double-centered EOF of GMST in seven NMME models and observations. The text box shows the correlation of the model's Niño-3.4 with the model's PCs. The observed values are in brackets for comparison.

	GMST-PC1($t+1$)	GMST-PC2($t+1$)
const	0.073*	-0.023
	(0.043)	(0.116)
GMST-PC1(t)	0.998***	-0.128
	(0.046)	(0.125)
GMST-PC2(t)	-0.041	-0.172
	(0.043)	(0.117)
N34-PC1(t+1)	0.281***	0.598***
	(0.043)	(0.117)
N34-PC2(t+1)	-0.068	0.135
	(0.043)	(0.117)
R-squared	0.924	0.448
R-squared Adj.	0.916	0.393
N	45	45

Standard errors in parentheses. * $p < .1$, ** $p < .05$, *** $p < .01$

Table S1. Regression results for the four-PC model

	GMST-PC1($t+1$)	GMST-PC2($t+1$)
const	0.074	-0.027
	(0.044)	(0.119)
GMST-PC1(t)	0.999***	-0.137
	(0.047)	(0.127)
N34-PC1(t+1)	0.281***	0.596***
	(0.044)	(0.119)
R-squared	0.918	0.396
R-squared Adj.	0.914	0.368
N	45	45

Standard errors in parentheses. * $p < .1$, ** $p < .05$, *** $p < .01$

Table S2. Regression results for the two-PC model

	GMST mean$(t+1)$	DC-PC1$(t+1)$
const	0.022*	-0.016
	(0.013)	(0.118)
GMST mean(t)	1.003***	-0.057
	(0.047)	(0.444)
Dec N34(t+1)	0.066***	0.525***
	(0.011)	(0.100)
R-squared	0.917	0.402
R-squared Adj.	0.913	0.374
N	45	45

Standard errors in parentheses. * $p < .1$, ** $p < .05$, *** $p < .01$

Table S3. Regression results for the simplified model.

	GMST mean$(t+1)$	DC-PC1$(t+1)$
const	0.022	-0.015
	(0.013)	(0.119)
GMST mean(t)	1.046***	0.331
	(0.052)	(0.461)
Dec rN34(t+1)	0.061***	0.519***
	(0.011)	(0.100)
R-squared	0.906	0.397
R-squared Adj.	0.902	0.368
N	45	45

Standard errors in parentheses. * $p < .1$, ** $p < .05$, *** $p < .01$

Table S4. Regression results for the simplified model using relative Niño-3.4.

Model	GMST level (°C decade^{-1})	Dec $N_{3.4}$ (°C decade^{-1})
COLA-RSMAS-CCSM4	0.25 [0.19, 0.28]	-0.09 [-0.54, 0.38]
COLA-RSMAS-CESM1	0.35 [0.31, 0.38]	0.09 [-0.43, 0.64]
CanESM5	0.30 [0.25, 0.33]	0.19 [-0.04, 0.46]
GEM5.2-NEMO	0.23 [0.19, 0.28]	0.20 [-0.16, 0.61]
GFDL-SPEAR	0.32 [0.28, 0.36]	0.06 [-0.30, 0.45]
NASA-GEOSS2S	0.26 [0.21, 0.31]	-0.28 [-0.81, 0.31]
NCEP-CFSv2	0.27 [0.23, 0.31]	-0.13 [-0.66, 0.37]
Observations	0.24 [0.20, 0.28]	-0.06 [-0.47, 0.38]

Table S5. Trends for June starts over the period 1991–2025. The 95% confidence intervals are computed by block bootstrap sampling over start years.

	Jun	Jul	Aug	Sep	Oct	Nov	Dec	Jan	Feb	Mar	Apr	May
Simplified + obs $N_{3.4}$ vs. Simplified + NMME $N_{3.4}$												
Wilcoxon	0.837	0.723	0.792	0.995	0.876	0.815	0.500	0.234	0.387	0.567	0.829	0.986
Sign test	0.885	0.804	0.939	0.995	0.696	0.568	0.568	0.568	0.696	0.696	0.696	0.939
Simplified + NMME $N_{3.4}$ vs. NMME GMST												
Wilcoxon	**0.045**	0.255	0.626	0.171	<**0.001**	0.107	0.176	0.336	0.480	0.289	0.289	0.745
Sign test	0.304	0.568	0.432	0.196	**0.001**	0.568	0.304	0.568	0.696	0.432	0.196	0.804

Table S6. Statistical significance of RMSE differences.